Journal of Aerospace Engineering
Volume 32, Issue 4, July 2019
10.1061/(ASC0E)AS.1943-5525.0001005

Degraded planary tracking control of an omni-directional vectored-thruster aerostat

Li Chen[1]; James F.Whidborne[2]; Qi Dong[3]; Dengping Duan[4]; Jinguo Liu[5]

Abstract

The problem of horizontal-plane tracking control of an omni-directional, four vectored-thruster aerostat when subjected to actuator failure is considered. The actuator failures result in the aerostat becoming underactuated, so it can only effect surge force and pure yaw moment about the body centre. To achieve accurate position control in the horizontal plane, direct position control is used instead of heading control.This mode of controller is called degraded tracking control in contrast to full authority control of the overactuated four vectored-thruster aerostat. This degraded tracking controller uses commanded yaw rate to track lateral position, and yaw moment to eliminate lateral position error, therefore yaw angle is not directly controlled. To guarantee the stability of the yaw motion, a Virtual Reference Point (VRP) tracking strategy is proposed, where the VRP is used instead of the body center (BC) in position tracking. The VRP generates a negative compensated force in the surge direction which makes the side-force and yaw moment have the same sign and so ensure that the aerostat is in a stable tracking configuration. Meanwhile the VRP also decreases the transmission ratio of commanded yaw rate to commanded lateral velocity, making the aerostat's yaw motion vary slowly during transitional phase, so steady position tracking is obtained.

[1]Researcher, School of Air Transportation, Shanghai University of Engineering Science, Shanghai, 201620, China; State Key Laboratory of Robotics, Shenyang Institute of Automation, Chinese Academy of Sciences, Shenyang, 110016, China.(corresponding author). Email:cl200432@tom.com
[2]Reader, Centre for Aeronautics, Cranfield University, Bedfordshire, MK43 0AL, United Kingdom. Email:j.f.whidborne@cranfield.ac.uk
[3]Research Engineer, Teaching and Research Section, MuDanJiang Medical University, Mudanjiang, 157400, China. Email:745890908@qq.com
[4]Professor, School of Aeronautics and Astronautics, Shanghai Jiao Tong University, Shanghai, 200240, P.R.China. Email:ddp@sjtu.edu.cn
[5]Researcher, State Key Laboratory of Robotics, Shenyang Institute of Automation, Chinese Academy of Sciences, Shenyang, 110016, China. Email:liujinguo@sia.cn

Keywords: vectored-thruster aerostat, degraded tracking control, underactuated, virtual reference point

Introduction

Given their hovering ability, static lift airships have been proposed as stratospheric (from 10km to 20km altitude) platforms (Smith et al. (2011); Yang and Liu (2018); Zhang et al. (2017)), the shape of the envelope has a major influence on an airship's performance(Khoury and Gillett (1999, p. 385)). The ellipsoidal shape displays a reduced lateral profile in crosswinds and has a higher lift efficiency. Therefore, this shape is advantageous for a platform hovering at a given altitude (Chen et al. (2016)). The efficiency of a conventional actuator, such as an aerodynamic control surface for stratospheric platforms is decreased by the low-atmospheric density and flight speed (Yang and Yan (2018); Azinheira et al. (2015); Yang and Yan (2016); Yang (2018)). One of the most effective substitutes is the vectored thruster (Rooz and Johnson (2005)). Thus a multi-thruster ellipsoidal aerostat is proposed for a stratospheric platform that hovers over a fixed area. The problem considered in this paper is the position tracking control of this aerostat subject to actuator failure.

The aerostat is rotationally symmetric with a height-to-diameter ratio of 0.6 and is shown in Fig. 1. It is equipped with four vectored propellers, each vectored propeller can change its thrust amplitude and direction independently. Hence under normal operation the vehicle is overactuated (Chen et al. (2015)) meaning that there may be more than one way to effect each Degree Of Freedom (DOF). In case of complete failure of a single thruster, the remaining thrusters can be reconfigured by using control allocation without having to change the motion controller structure provided full controllability is guaranteed (Chen et al. (2016)).However if two or more thrusters totally fail then the aerostat changes from being overactuated to underactuated. Hence the controller must be redesigned to maintain tracking control. This is termed *degraded control* as compared to the fully-actuated situation.

Literature dealing with the control of underactuated vehicles is fairly extensive and ever growing. For control in the horizontal plane, most of the study has been devoted to surface marine vehicles, but here this is extended to the aerostat problem. The concepts proposed for solving such 3DOF state control problems with two control inputs can be divided into two notably different strategies: full 3 DOF state control and reduced 2 DOF state control (Breivik (2003)). Using only 2 control inputs to control the full 3 DOF means that it is an underactuated control problem. Since the stabilization problem system does not satisfy Brockett's condition (Brockett (1983)), a smooth,

time-invariant, state feedback control algorithm cannot be utilized for stabilization to a set-point (Pettersen and Fossen (2000); Do et al. (2002); Zheng et al. (2013, 2016)). Lowering the output space from full 3 DOF to reduced 2 DOF ensures that the control problem is no longer of an underactuated character. Hence ordinary smooth, static state feedback control laws can be employed for both trajectory tracking and stabilization to a fixed point. However, for this approach to be successful, the strategy employed must ensure indirect control of the underactuated state such that it behaves as desired (Godhavn et al. (1998); Morel and Leonessa (2002); Consolini and Tosques (2012); Toussaint et al. (2000)).

Conventional 2 DOF state controllers for underactuated ships do not control the vehicle's position directly, but indirectly via the heading (Pettersen and Fossen (2000); Lauvdal and Fossen (1997); Lekkas and Fossen (2012)). If there are external disturbances due to wind, the ship's position will not follow the desired track. To overcome this problem, direct position control was proposed instead of the heading control for underactuated vehicles (Godhavn (1996); Berge et al. (1999); Ashrafiuon et al. (2008); Fossen et al. (1998)). The strategy is to prove the exponential convergence of the body-fixed position and velocity errors while the heading loop is open and hence it is referred to as the internal states (Godhavn et al. (1998)). The stability of the internal dynamics depends mainly on the damping terms in yaw, so it can be unstable for some ships, in fact the ship may rotate a full 180 degrees (Fossen et al. (1998)). This will happen for the aerostat considered here because of its rotationally symmetric shape, it has a smaller yaw damping coefficient than that of aerostats with a 'teardrop' shape, so it is easy to change heading under disturbance.

A Virtual Reference Point (VRP) tracking strategy was originally proposed for tanker control by (Pinkster and Marin (1986)). In this method the VRP is used instead of the body center (BC) in position tracking. The VRP tracking strategy extends the BC controller to provide position tracking with increases yaw damping and stable internal dynamics (Morel and Leonessa (2010)). Furthermore the concept possesses an inherent weather-vaning property (Godhavn et al. (1998)), making it very interesting for application to control of this aerostat.In this paper the VRP is also adopted to design a direct position 2 DOF state controller for the aerostat when subjected to failure of two opposite thrusters, and the mechanism of VRP for stability of set-point tracking is investigated.

The paper is structured as follows. Section "Airship dynamic model" begins by introducing the aerostat model. Section "Degraded tracking control law" details the controller design, which is divided into two parts. First, the

design of the position controller based on VRP is considered; then the same controller is calculated based on BC, the difference of two controller in terms of its force magnitude are calculated. The performance of the VRP controller is then tested by simulation in Section "Application to the aerostat model". The internal dynamic stability is analyzed and the mechanism of VRP in steady position tracking is investigated in Section "Internal dynamics stability". Section "Conclusion" concludes the paper with some observations.

Airship dynamic model

A aerostat with a diameter of 6 m and volume of 70 m^3 is taken for controller design. The gondola is suspended under its body to increase pitch and roll stability as shown in Fig. 1.

Fig. 1. Overall structure of the aerostat

Suppose that the aerostat is subject to a serious actuator fault whereby two opposite thrusters fail totally. The working pair are located on opposite sides of the aerostat. The control inputs from the two propellers can only provide a surge motion and yaw rotation. So the 3 DOF horizontal dynamic model is considered. The body-fixed frame is established as shown in Fig. 2.

The full 6 DOF non-linear dynamics can be found in Chen et al. (2015). If we assume that excursions in roll, pitch and heave are small, then the simplified horizontal plane 3 DOF dynamics that are used for the controller design are described by

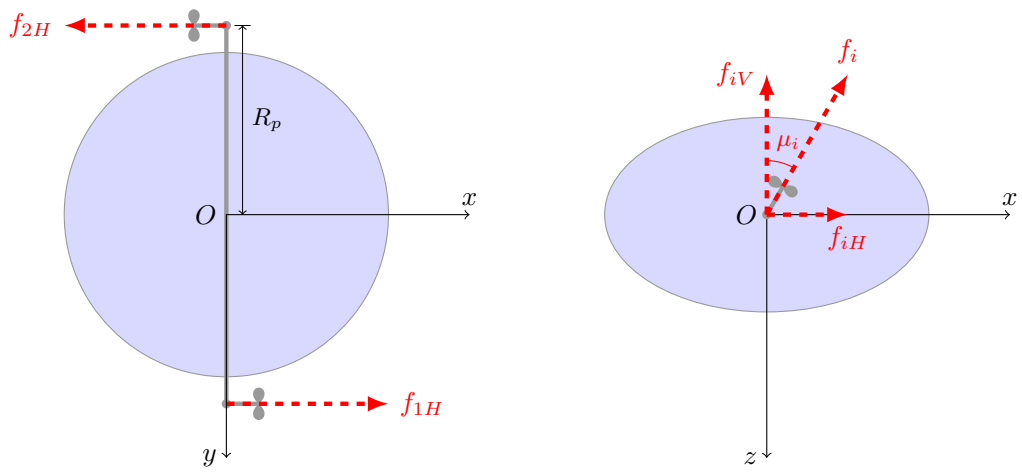

Fig. 2. Body-fixed frame and vectored-thrust decomposition

$$(m + m_{11})\dot{u} = (m + m_{22})vr + F_{A1} + F_{T1} \tag{1}$$

$$(m + m_{22})\dot{v} = -(m + m_{11})ur + F_{A2} \tag{2}$$

$$(I_z + m_{66})\dot{r} = (m_{11} - m_{22})wv + F_{A6} + F_{T6} \tag{3}$$

where u, v, r are the state variables, respectively forward velocity, lateral velocity and yaw rate, m is the mass of aerostat, m_{11}, m_{22}, m_{66} are the virtual masses and inertia of the aerostat along the u, v and r directions respectively, I_z is the moment of inertia of the aerostat in yaw direction, and the external forces consist of aerodynamic forces, F_{Ai}, and vectored thrusts, F_{Ti}, for $i = 1, 2, 6$.

The vectored angle of each propeller is denoted by μ_1 and μ_2, and the generated force is represented by f_1 and f_2. In the vectored-rotation plane,which is parallel to the Oxz plane, each vectored thrust is decomposed into two orthogonal forces f_{iH} and f_{iV}, $i = 1, 2$, where $f_{iH} = f_i \sin(\mu)$, $f_{iV} = f_i \cos(\mu)$. These decomposed pairs are then

resolved into the body-fixed frame along the x-, y-, and z-axes with matrix $\mathbf{B}$ in the 6 DOF model as

$$\mathbf{F_T} = \mathbf{Bu} = \begin{pmatrix} 1 & -1 & 0 & 0 \\ 0 & 0 & 0 & 0 \\ 0 & 0 & -1 & -1 \\ 0 & 0 & R_p & -R_p \\ 0 & 0 & 0 & 0 \\ -R_p & -R_p & 0 & 0 \end{pmatrix} \begin{pmatrix} f_{1H} \\ f_{2H} \\ f_{1V} \\ f_{2V} \end{pmatrix} \tag{4}$$

where R_p is the arm-length of the propeller effector on the body frame as shown in Fig. 2, and $\mathbf{B}_2$ is the reduced input matrix $\mathbf{B}$ for 3 DOF planar model with

$$\mathbf{B}_2 = \begin{pmatrix} 1 & -1 & 0 & 0 \\ 0 & 0 & 0 & 0 \\ -R_p & -R_p & 0 & 0 \end{pmatrix} \tag{5}$$

From $\mathbf{B}$ in equation (4), we can see that the thrusters also affect the vertical and roll motion while driving the movement in the horizontal plane. Hence the simulations in section are conducted with the full 6 DOF non-linear model.

Because of the rotational symmetry of the aerostat body and the symmetrical installation of propellers, there is no fundamental distinction between forward and backward travel. As shown in Fig. 2, the bow direction of the aerostat could be defined as any of positive x-direction, negative x-direction, positive y-direction or negative y-direction all in the body frame.

Degraded tracking control law

For accurate position tracking, the position tracking error is directly considered in the controller design. The longitudinal position is controlled by the forward thrust and the lateral position is controlled by commanded yaw rate $\tilde{r}$ according to equation (2). Since the yaw moment is used to control yaw rate which is directly related to the lateral position error, the yaw angle is not independently controlled as it follows the yaw rate passively. Such

situations may occur if yaw damping coefficient is not large enough to stabilize the yaw rate and the aerostat may turn around and lead with the stern. According to Godhavn et al. (1998), to solve this problem a VRP, $\mathbf{P_v}$, is chosen as the position output point and is placed on the aerostat's longitudinal symmetry axis at a positive distance d_u from the body centre (BC) as shown in Fig. 3. Note that if $d_u = 0$ then the VRP controller reduces to the BC controller.

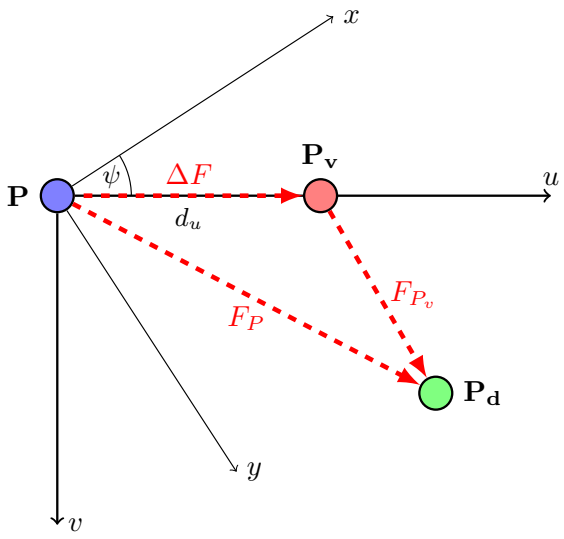

Fig. 3. Forces analysis in tracking

Assuming the desired output to the system is $\mathbf{P_d} = [x_d, y_d]^{\mathrm{T}}$, the current position is $\mathbf{P} = [x, y]^{\mathrm{T}}$ and the virtual reference point is forward located at $\mathbf{P_v} = [x_v, y_v]^{\mathrm{T}}$, the relation between reference point and the current point is given by

$$\mathbf{P_v} = \mathbf{P} + \mathbf{R} \begin{bmatrix} d_u \\ 0 \end{bmatrix} \tag{6}$$

where $\mathbf{R}$ is the transformation matrix

$$\mathbf{R} = \begin{pmatrix} \cos(\psi) & -\sin(\psi) \\ \sin(\psi) & \cos(\psi) \end{pmatrix} \tag{7}$$

The linear velocity controller from $\mathbf{P_v}$ to $\mathbf{P_d}$ is set as

$$\mathbf{v}_c = \mathbf{R}^{\mathrm{T}} \mathbf{k} (\mathbf{P_d} - \mathbf{P_v}) \tag{8}$$

where $\mathbf{v_c} = [u_c, v_c]^{\mathrm{T}}$ is the commanded velocity vector for set-point tracking and $\mathbf{k} = \mathrm{diag}[k_1, k_2]$ is a designed positive vector. The linear acceleration controller is set as

$$\dot{\mathbf{v}}_\mathbf{c} = \lambda(\mathbf{v_c} - \mathbf{v}) \tag{9}$$

where $\dot{\mathbf{v}}_\mathbf{c} = [\dot{u}_c, \dot{v}_c]$ is the commanded acceleration vector for commanded velocity tracking and $\lambda = \mathrm{diag}[\lambda_1, \lambda_2]$ is a designed positive vector. Substituting equations (6) and (8) into equation (9), we get

$$\begin{aligned}
\dot{\tilde{u}}_c =& \lambda_1[(k_1(x_d - x)\cos(\psi) + k_2(y_d - y)\sin(\psi)) \\
& - (k_1 d_u(\cos(\psi))^2 + k_2 d_u(\sin(\psi))^2) - u] \\
\dot{\tilde{v}}_c =& \lambda_2[(-k_1(x_d - x)\sin(\psi) + k_2(y_d - y)\cos(\psi)) \\
& + (k_1 d_u \cos(\psi)\sin(\psi) - k_2 d_u \cos(\psi)\sin(\psi)) - v]
\end{aligned} \tag{10}$$

For the lateral position tracking, we use the dynamic relationship from equation (2)

$$r_c = \frac{f_{A2} - (m + m_{22})\dot{\tilde{v}}_c}{(m + m_{11})u} \tag{11}$$

$$\dot{\tilde{r}}_c = \lambda_3(r_c - r) \tag{12}$$

where r_c is the commanded yaw rate, $\dot{\tilde{r}}_c$ is the commanded yaw acceleration, and λ_3 is a positive designed number. To avoid a singularity in the calculation of r_c when $u = 0$, we use a threshold variable u_p to replace u in equation (11):

$$u_p = \begin{cases} 0.5, & \text{for } 0 \le u \le 0.5 \\ u, & \text{for } |u| > 0.5 \\ -0.5, & \text{for } -0.5 \le u < 0 \end{cases} \tag{13}$$

Finally we apply feedback linearization to the system given by equations (1) – (3) to achieve station-keeping tracking

control forces

$$\begin{aligned} F_{T1} &= (m + m_{11})\dot{\tilde{u}}_c - (m + m_{22})vr - F_{A1} \\ F_{T6} &= (I_z + m_{66})\dot{\tilde{r}}_c - (m_{11} - m_{22})wv - F_{A6} \end{aligned} \tag{14}$$

Inserting equation (10) into (14), the final control forces are written as

$$\begin{aligned} F_{T1} =& (m + m_{11})\lambda_1(k_1(x_d - x)\cos(\psi) + k_2(y_d - y)\sin(\psi) \\ & - k_1 d_u(\cos(\psi))^2 - k_2 d_u(\sin(\psi))^2 - u) - (m + m_{22})vr - F_{A1} \\ F_{T6} =& (I_z + m_{66})\lambda_3 \left(\frac{F_{A2} - (m + m_{22})\dot{\tilde{v}}_c}{(m + m_{11})u_p} - r \right) - (m_{11} - m_{22})wv - F_{A6} \end{aligned} \tag{15}$$

where these controllers guarantee convergence of x to x_d and y to y_d respectively. The control forces are related with the commanded accelerations as shown in equation (14). With the position relationship of $\mathbf{P_v}$ with $\mathbf{P}$, the tracking acceleration $[\dot{\tilde{u}}_c^{'}, \dot{\tilde{v}}_c^{'}]^{\mathrm{T}}$ of $\mathbf{P}$ can also be deduced from equation (10) as

$$\begin{aligned} \dot{\tilde{u}}_c &= \dot{\tilde{u}}_c^{'} - \lambda_1(k_1 d_u(\cos(\psi))^2 + k_2 d_u(\sin(\psi))^2) \\ \dot{\tilde{v}}_c &= \dot{\tilde{v}}_c^{'} + \lambda_2(k_1 d_u \cos(\psi)\sin(\psi) - k_2 d_u \cos(\psi)\sin(\psi)) \end{aligned} \tag{16}$$

If we choose $k_1 = k_2$, then equation (16) can be simplified to

$$\begin{aligned} \dot{\tilde{u}}_c &= \dot{\tilde{u}}_c^{'} - \lambda_1 k_1 d_u \\ \dot{\tilde{v}}_c &= \dot{\tilde{v}}_c^{'} \end{aligned} \tag{17}$$

So the difference in choosing different tracking output point is just the different control force acting on the aerostat as shown in Fig. 3, i.e. $\mathbf{F_p} = \mathbf{F_{P_v}} + \Delta\mathbf{F}$, and $\Delta\mathbf{F} = [\Delta F_{T1}, \Delta F_{T6}]^{\mathrm{T}}$ is called the compensated force where

$$\Delta\mathbf{F} = \begin{bmatrix} -(m + m_{11})\lambda_1(k_1 d_u(\cos(\psi))^2 + k_2 d_u(\sin(\psi))^2) \\ -(I_z + m_{66})\lambda_3 \frac{(m+m_{22})\lambda_2(k_1 - k_2)d_u \cos(\psi)\sin(\psi)}{(m+m_{11})u_p} \end{bmatrix} \tag{18}$$

The overall control structure is as shown in Fig. 4.

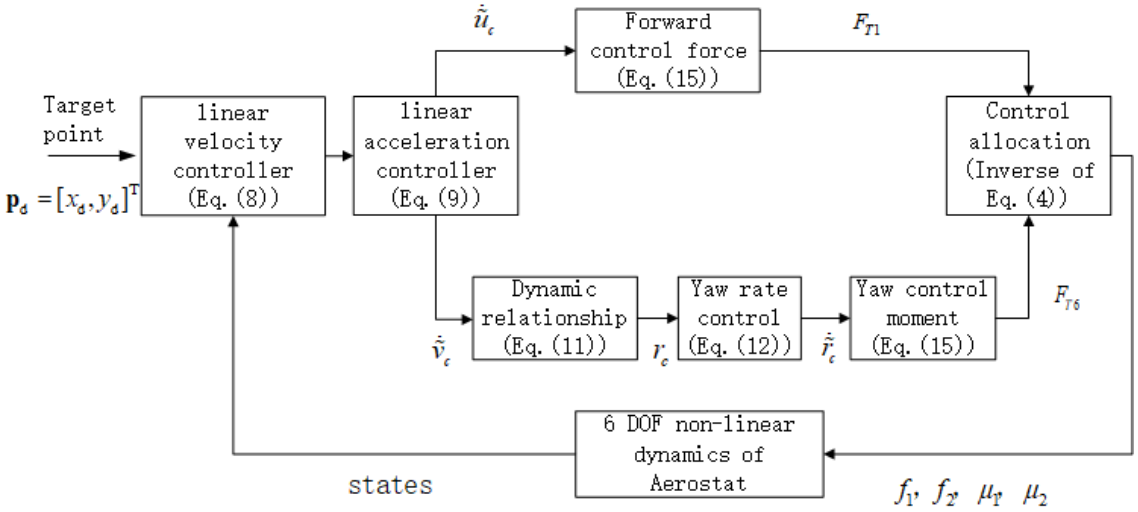

Fig. 4. Overall structure of controller

Application to the aerostat model

In this section we present two simulation cases for set-point tracking control: in the first case the body centre is taken as the output tracking point (BC case), and in the second case the VRP is taken as the output tracking point (VRP case). The difference between the two cases is just the magnitude of compensated force as shown in equation (18). Here $d_u = 5$ is set and the desired position is $P_d = [30, 30]^{\mathrm{T}}$.The value of d_u is chosen as a compromise between yaw damping, which increases with d_u, and tracking accuracy, which decreases. In order to achieve different destination points, we construct two second order command filters for x and y position tracking: $\ddot{n}_c + 2\zeta\omega\dot{n}_c + \omega^2 n_c = \omega^2 n_d$, where n_d is the reference set-point input, $n_c = [x_c, y_c]^{\mathrm{T}}$ is the tracking trajectory output. The relative damping is chosen as $\zeta = 1$, and the natural frequency is chosen as $\omega = 0.1$ rad/s which is based on the open loop dynamics model for a given trim velocity. The controller parameters are chosen as $k_1 = 0.1$, $k_2 = 0.05$, $\lambda_1 = 0.5$, $\lambda_2 = 1$ and $\lambda_3 = 0.5$.

Comparison of different output points

The simulation results for the BC case are shown in Figs 5-8, and Figs 9-12 show those for the VRP case.

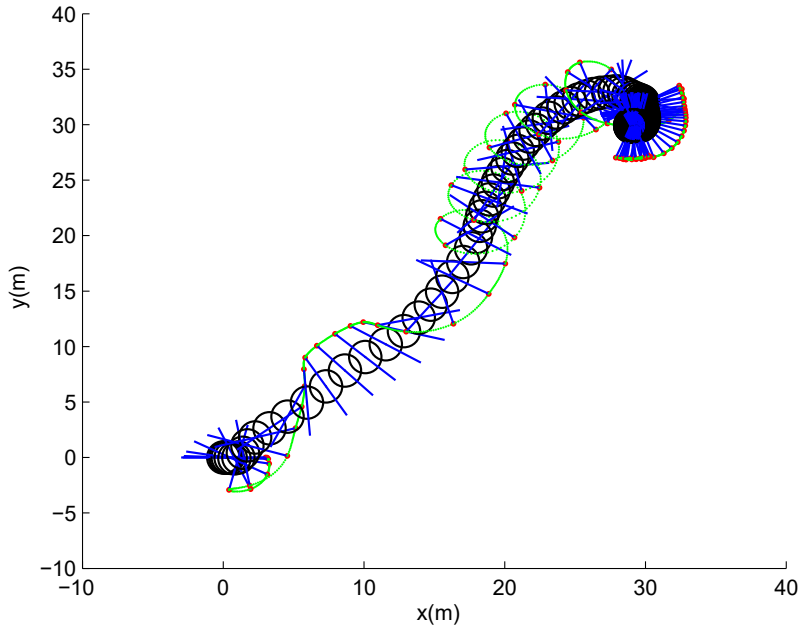

Fig. 5. Tracking trace in BC case (black circles denote the aerostat body, blue lines denotes the direction of the aerostat, the red points are the aerostat's bow and the green line indicates the trajectory of the aerostat's bow)

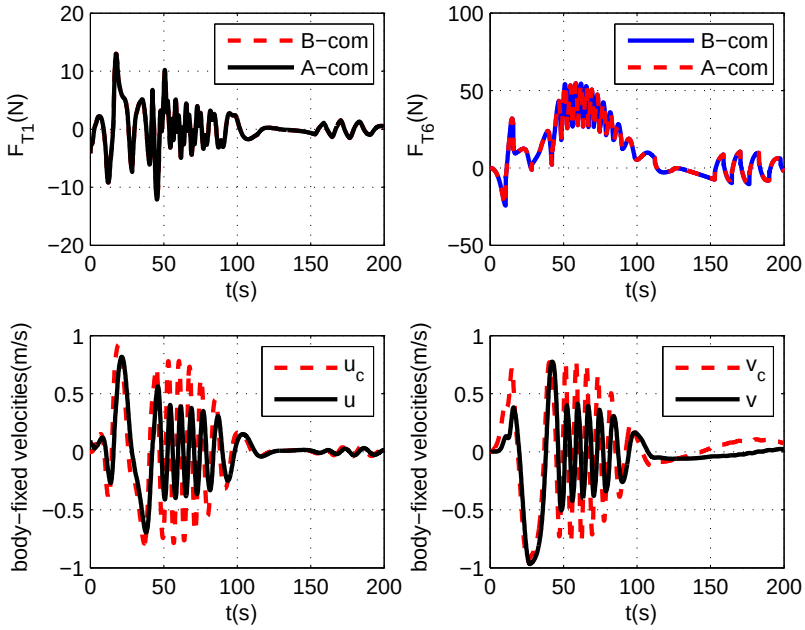

Fig. 6. Force and body-fixed velocity in BC case (B-com means without force compensation and A-com means with force compensation)

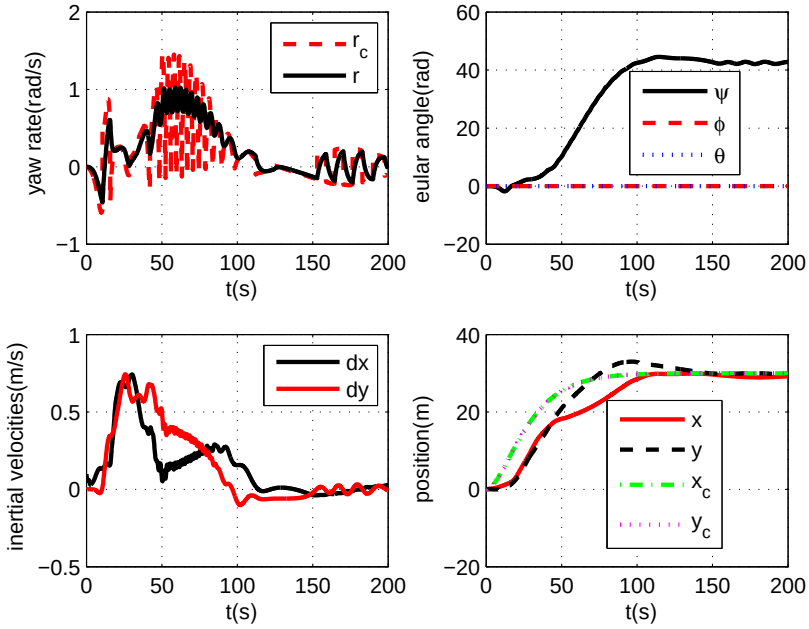

Fig. 7. Yaw and inertial velocity in BC case, where dx,dy are inertial velocities

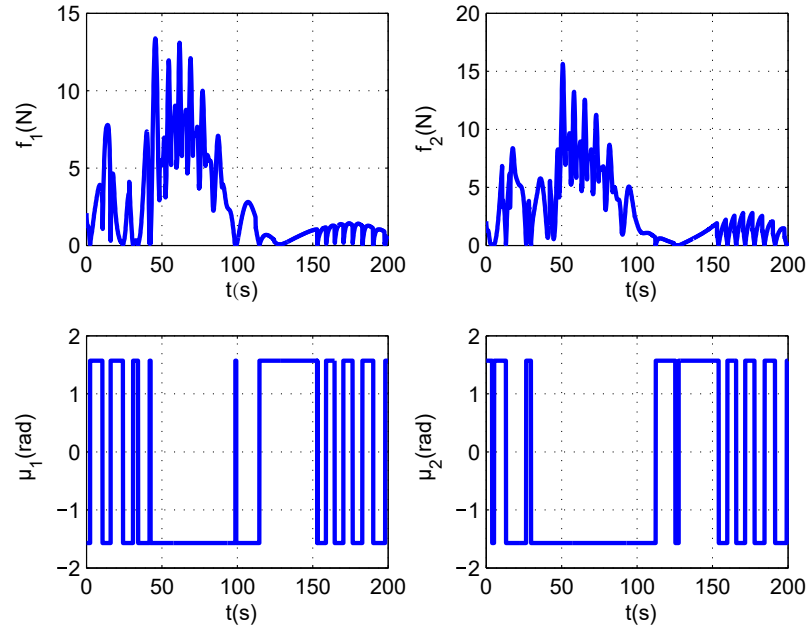

Fig. 8. Thrust and vectored angle of two thrusters in BC case

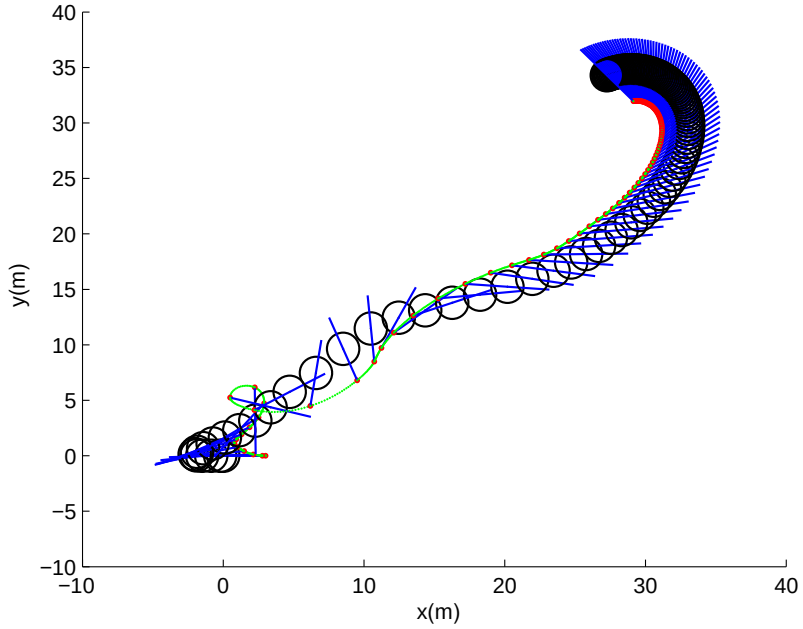

Fig. 9. Tracking trace in VRP case (black circles denote the aerostat body, blue lines denotes the direction of the aerostat, the red points are the aerostat's bow and the green line indicates the trajectory of the aerostat's bow)

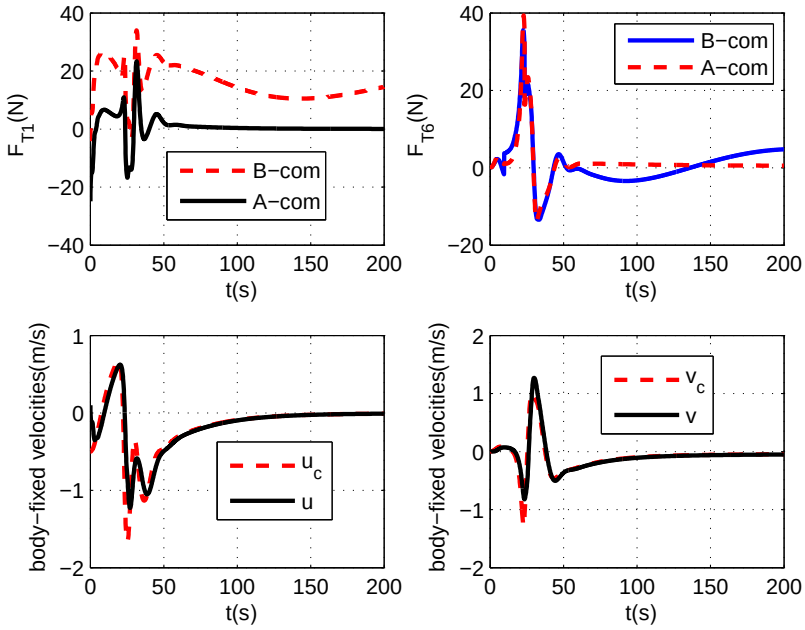

Fig. 10. Force and body-fixed velocity in VRP case (B-com means without force compensation and A-com means with force compensation)

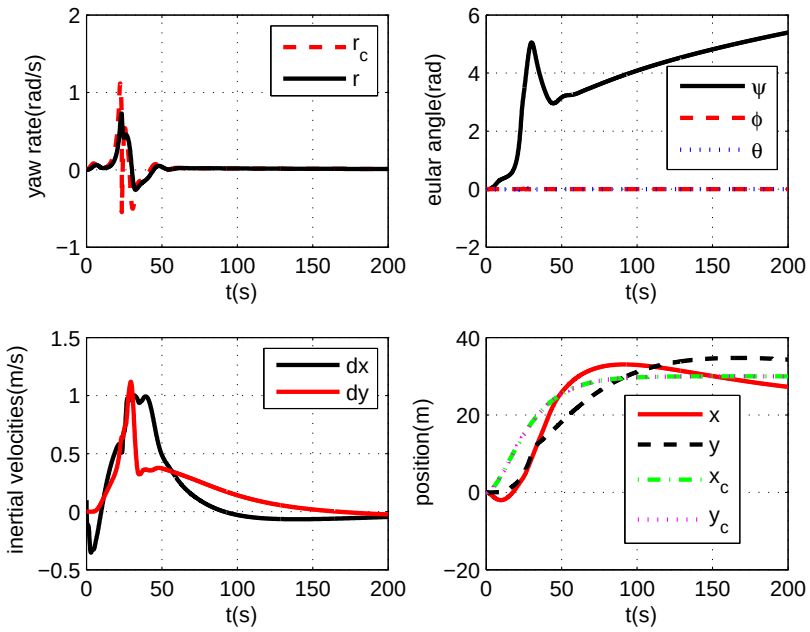

Fig. 11. Yaw and inertial velocity in VRP case, where dx,dy are inertial velocities

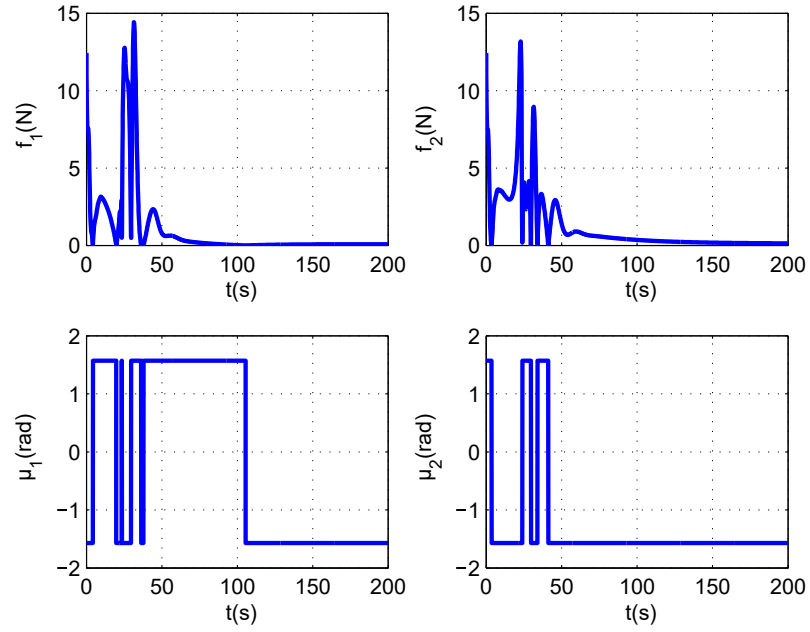

Fig. 12. Thrust and vectored angle of two thrusters in VRP case

Comparing the set-point tracking results of the two cases in Figs 5 and 9, we can conclude that both methods can achieve set-point tracking, however the variation of the heading angles are very different. During the transient

process until about 100s the yaw rate in the BC case varies constantly and the aerostat rotates until a final stable heading of about 40 rad as shown in Fig. 7. The green line in Fig. 5 is the trajectory of the aerostat's bow which shows the rotation. The yaw rate in the VRP case also varies during in the transient process, however with smaller amplitude and shorter transient time, with a single rotation of the aerostat resulting in a final stable heading of about 4 rad as shown in Fig. 11. The green line in Fig. 9 shows the change of the aerostat's heading. The aerostat travels to the destination almost backwards, thanks to the symmetric configuration of two vectored thrusters of the symmetrical aerostat. Due to the symmetry, it matters little for this aerostat whether it travels forwards or backwards.

Further we look into the control force and velocity responses for the two cases. We find that in the BC case there is no compensated force, so there is no difference between B-com and A-com in Fig. 6. However in the VRP case there is a large negative compensated force in surge and a small amount of yaw moment in Fig. 10. With the compensated force, the body-fixed velocities and the inertial velocities in the tracking phase are smoother and more stable compared with those in the BC case as shown in Figs 7 and 11. Because of the extra negative force in the VRP case, the body-fixed velocity u is negative most of the time as shown in Fig. 10, and that of the BC case oscillates between positive and negative as shown in Fig. 6.

The real actuator outputs of the two cases are shown in Figs 8 and 12. In the VRP case the outputs of each thruster are better with less switching compared with those of the BC case. Note that the vectored thrusters switch between +90 and -90 degrees, these being the angles that provide maximum lateral thrusts in the Oxz pane.

There are tracking errors in both x and y direction in the VRP case as seen in Fig. 11. This is because the VRP is taken as the tracking output point, so the Euclidean norm of the position error is just the distance from reference point to the body centre, satisfying that $\|\mathbf{P_d} - \mathbf{P}\|_2 = \mathrm{d_u}$, so the VRP tracking is a bounded-error method.

Performance analysis

To validate the set-point tracking ability of the VRP method, Fig. 13 illustrates the aerostat trajectories to different destinations in the four quadrants of the Oxy-plane. Fig. 14 shows the heading and velocity. The set-points in these different locations are reached. There is always extra negative compensated force in the surge direction, so the body-fixed velocity u is negative during most of the tracking period as shown in Fig. 14. This is

really the key factor for stabilizing the heading angle in set-point tracking, and will be further discussed in the next section.

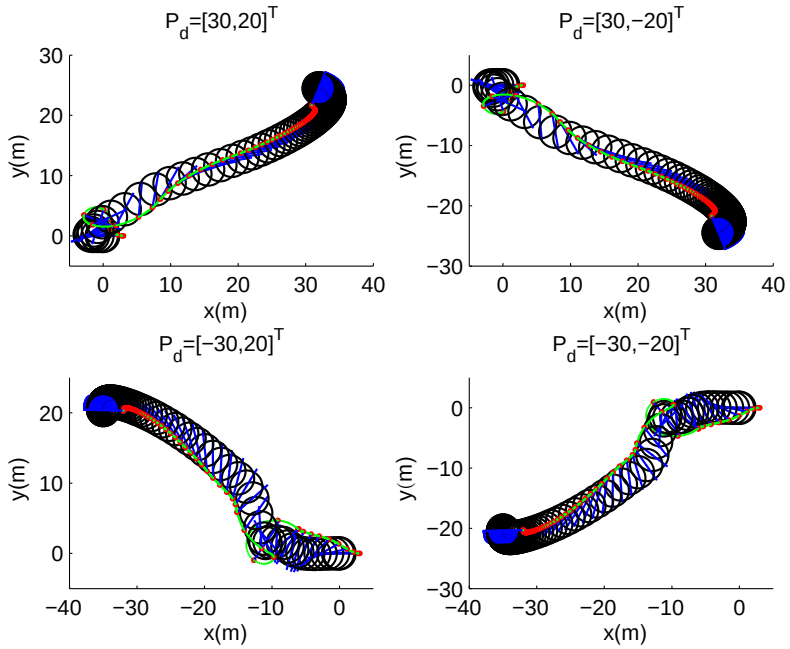

Fig. 13. Tracking trace of different set-points

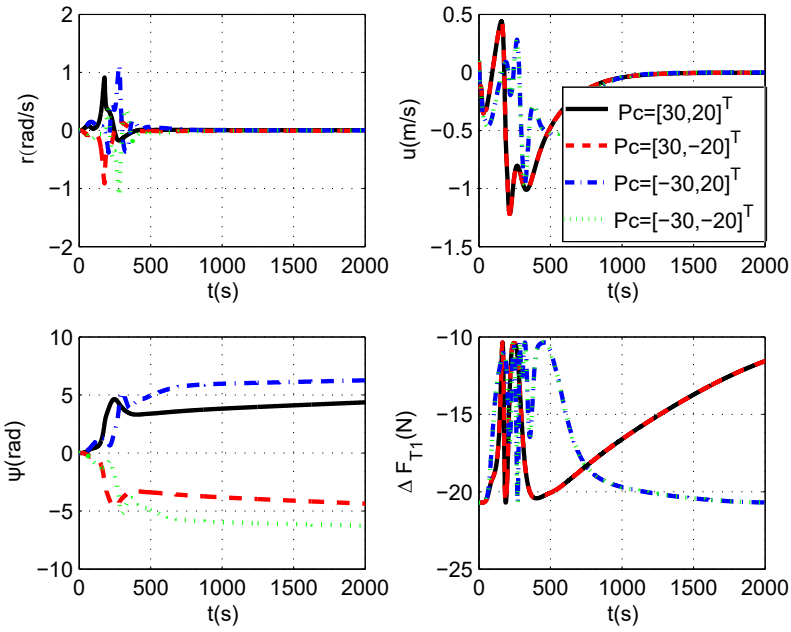

Fig. 14. Yaw and velocity of different set-points

As mentioned in Section "Introduction", one of the advantages in the proposed degraded tracking controller is the use of direct lateral position control instead of the heading control and this improves the tracking accuracy under external disturbances, such as wind. Here different simulations in wind fields are performed to validate the tracking ability in wind.For comparison, the conventional 2 DOF state controller with VRP is designed which does not control the vehicle's position directly, but indirectly via the heading. Figs 15 and 16 illustrate the position tracking ability of two methods in a relatively strong wind field compared with the inertial tracking velocity. The aerostat is controlled towards a fixed planar point $\mathrm{P_d} = [30\mathrm{m}, 30\mathrm{m}]$ in different wind conditions: no wind $\mathrm{Wd} = [0, 0]$, steady lateral wind $\mathrm{Wd} = [0, 2\mathrm{m/s}]$ and steady longitudinal wind $\mathrm{Wd} = [2\mathrm{m/s}, 0]$. From Fig. 15 we can see that the tracking trajectories are largely determined by the wind with conventional method, and there are large deviations from the destination. However, with the direct position VRP controller, the aerostat has a relatively stable tracking process and there is little difference from the destination with the different wind fields as shown in Fig. 16. So the VRP method has good performance in steady wind with the direct lateral position control.

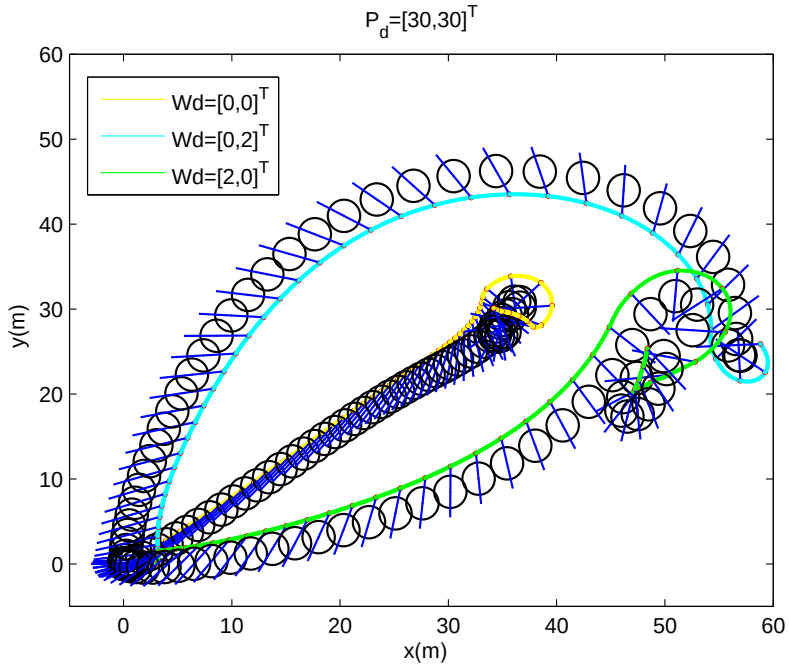

Fig. 15. Trajectories of conventional controller under different wind fields

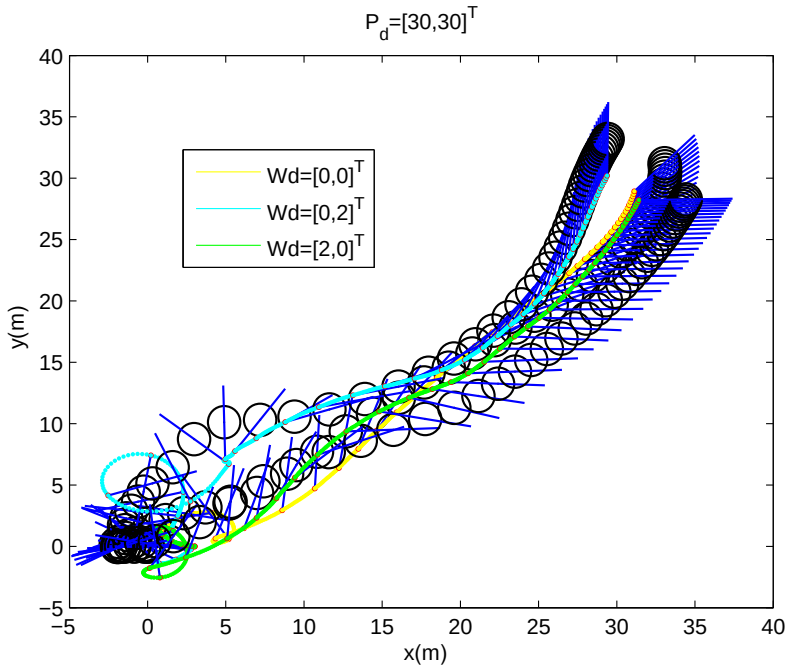

Fig. 16. Trajectories of direct position controller under different wind fields

Internal dynamics stability

The trajectory tracking problem for underactuated surface ship has generated great interest in the literature (Godhavn et al. (1998); Morel and Leonessa (2002); Consolini and Tosques (2012); Toussaint et al. (2000); Morel and Leonessa (2010)). Accordingly, the control design objective for such a nonminimum-phase system should not be perfect tracking, but bounded-error tracking (Slotine and Li (1991); Leonessa et al. (2006)). One approach consists of choosing the VRP as the tracking output to remove the nonminimum-phase behavior (Godhavn et al. (1998); Morel and Leonessa (2002); Consolini and Tosques (2012)). The stability of the internal dynamics was indirectly demonstrated through numerical simulation (Consolini and Tosques (2012); Berge et al. (1999); Morel and Leonessa (2010)) or analytic results can be obtained based on linearization or some constrained conditions (Morel and Leonessa (2002); Fossen et al. (1998); Leonessa et al. (2006))

In this section we discuss the VRP mechanism for guaranteeing stable tracking based on the nonlinear model. This investigation is conducted in two different ways. The first is to guarantee a stable tracking configuration, the other is to decrease the transmission ratio between yaw rate and lateral velocity.

Stable tracking configuration

According to Lekkas and Fossen (2012), if the side force and yaw moment have the same sign in the inertial frame then the ship will not rotate around in position tracking. This is the same situation for the aerostat, we refer to it as the stable tracking configuration. The first contribution of the VRP is to provide the stable tracking configuration under the failure cases. Without loss of generality, when the lateral aerodynamics f_{A2} is neglected, equation (11) can be simplified to

$$r_c = \frac{-(m + m_{22})\dot{\tilde{v}}_c}{(m + m_{11})u} \tag{19}$$

To make the side force and yaw moment have the same sign in the initial configuration, r_c should follow the $\dot{v}_c$ in the same direction and the only way to satisfy this condition is that $u < 0$. This is true in Fig. 14, in the steady tracking phase the body-fixed u varied from the negative to zero. It is the compensated force in equation (18) that makes u negative. Here for simplification we choose the controller parameter $k_1 = k_2$. Then in equation (18), only the forward compensated force is left $\Delta F_{\mathrm{T1}} = -(m + m_{11})\lambda_1 k_1 d_u$, and it is always negative and with amplitude determined by the distance from VRP to BC, d_u.

Figures 17 and 18 show details of the initial response to analyse the mechanism of the yaw movement. At the beginning of tracking, $v_c > 0$ and $\dot{\tilde{v}}_c > 0$, however u_c has a complicated movement as shown in Fig. 17. First, because u_p is used instead of initial value $u = 0$ in equation (11), so $u_p > 0$, which makes r_c negative. Soon after, because of the negative compensated force created, the aerostat moves backwards with $u < 0$ and $r_c > 0$ too. Furthermore because of the command filter, described in the start of Section 4, $x_c(t) < \mathrm{d_u}$ at the beginning (0–7s), both make u_c negative, so the aerostat is in a stable tracking configuration, even though x moves to the opposite direction. Later, when $x_c(t) > \mathrm{d_u}$, then $u_c > 0$ (7.7s, $\psi = 0.247$ rad) as shown in Fig. 18, r_c becomes negative, i.e. has an opposite sign to $\dot{\tilde{v}}_c$, so the aerostat is in an unstable tracking configuration. Because of the light yaw damping of this aerostat, its heading changes very quickly. The heading tends to go back until it reaches $\psi = 2.61$ rad (23.5 s) as shown in Fig. 17, and u_c becomes negative again, and then $u < 0$, $r_c > 0$ and $\dot{\tilde{v}}_c > 0$, so the aerostat is in a stable situation again, and the normal tracking process begins. During this transient process, the heading is already in the location of $\psi = 2.61$ rad and $r = 0.722$ rad/s. After that the stability condition is satisfied, so the aerostat moves to the destination backwards.

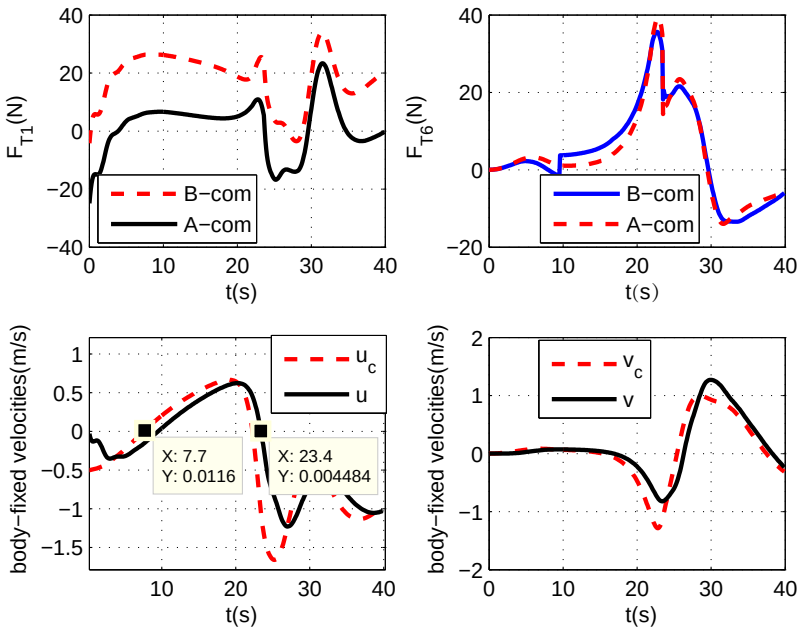

Fig. 17. Force and body-fixed velocity in VPR case (in details)

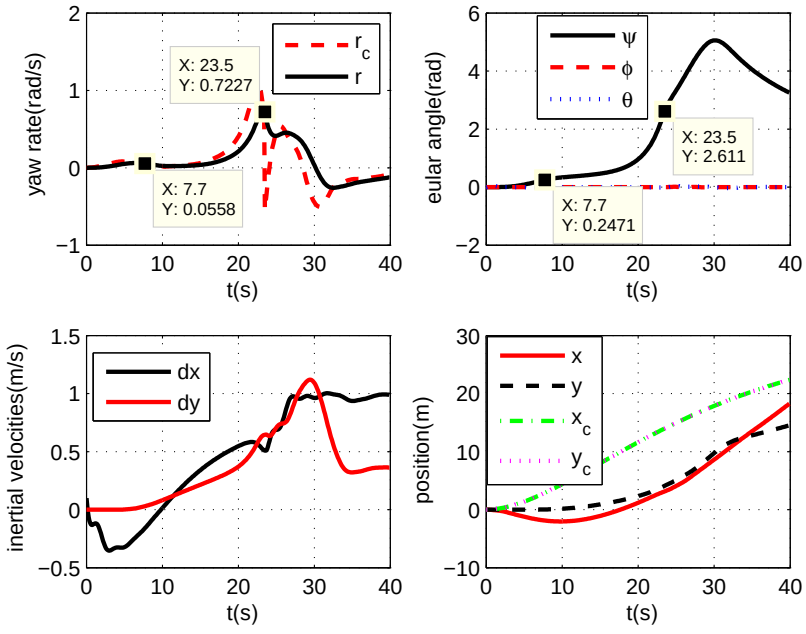

Fig. 18. Yaw and inertial velocity in VPR case, where dx,dy are inertial velocities(in details)

However for the BC case shown in Fig. 6, for the initial few seconds $u_c > 0$ and the aerostat is in an unstable situation. Then with the change of ψ, there is a period for which $u < 0$, however this is too brief and lacks a

negative compensated force. Then ψ reaches a new position and u becomes positive again. This is repeated along the whole trajectory resulting in oscillation, especially near to the destination as shown in Fig. 5.

Reduction of the transmission ratio between yaw rate and lateral velocity

The second contribution of the VRP is to decrease the transmission ratio of commanded yaw rate r_c to commanded lateral velocity v_c. The transmission coefficient is shown in equation (19) and the relationship $u_c = u_c^{'} - k_1 d_u$ can be deduced from equation (8). For a stable tracking configuration the longitudinal velocity should satisfy $u < 0$, so the commanded velocity $u_c < 0$ or $u_c^{'} < 0$. Because $k_1 > 0$ and $d_u > 0$, o we have $|u_c| > |u_c^{'}|$, that is to say with the VRP, the transmission ratio is smaller than that without VRP. So for a given lateral command, a smaller yaw rate command is required, so the yaw movement during transient tracking is smaller. So the VRP decreases the transmission ratio of commanded lateral velocity v_c to commanded yaw rate r_c during the transitional phase, and as such prevents the yaw divergence in the tracking process.

As mentioned in section , the Euclidean norm of the position tracking error is just the distance from VRP to the BC. So there is a trade-off between the tracking accuracy and the yaw divergence in choosing the magnitude of d_u.

Conclusion

The degraded tracking control of a multi-thruster aerostat in an underactuated situation is proposed. For more accurate position tracking, lateral position control is used instead of heading control. The lateral position is controlled by yaw rate through yaw moment, therefore yaw angle is only controlled indirectly. In this method the VRP is used instead of the BC in position tracking. The VRP tracking strategy extends the BC controller to provide position tracking with increases yaw damping and stable internal dynamics.

The VRP mechanism is investigated based on the nonlinear model in terms of keeping the stable tracking configuration and decreasing the transmission ratio of commanded yaw rate to commanded lateral velocity. The approach can achieve arbitrary set-point tracking with bounded error. To validate the capability of the VRP based direct position controller in a constant wind, a conventional 2 DOF state controller is designed for comparison. Simulation results illustrate the position tracking ability of this method in a wind field.

The simulation results show that there are periods during which the aerostat turns and travels almost backwards. This is not a concern for this particular application due to the symmetry of the aerostat, however, to extend the approach to other aerostat configurations and shapes requires further study.

Acknowledgements

This work is supported by the National Science Foundation of China, No. 61733017, and by the Foundation of State Key Laboratory of Robotics of China, No. 2018O13, also sponsored by Shanghai Pujiang Program, No. 18PJD018.

References

Ashrafiuon H, Muske KR, McNinch LC, Soltan RA. Sliding-mode tracking control of surface vessels. *IEEE Transaction on Industrial Electronics*. 2008, 55(11):4004–4012.

Azinheira JR, Moutinho A, Carvalho JR. Lateral control of airship with uncertain dynamics using incremental nonlinear dynamics inversion. *IFAC-PapersOnLine*. 2015, 48(19):69–74.

Berge SP, Ohtsu K, Fossen TI. Nonlinear control of ships minimizing the position tracking errors. *Modeling, Identification and Control*. 1999, 20(3):177–187.

Breivik M. Nonlinear maneuvering control of under-actuated ships. *Masters Thesis, Norwegian University of Science and Technology*. 2003.

Brockett RW. Asymptotic stability and feedback stabilization. In *Differential Geometric Control Theory*. (Brockett RW, Millman RS, Sussmann HS, eds.), Birkhäuser, Boston, MA, 1983:181–191.

Chen L, Wen YB, Zhou H, Duan DP. Design and control of a multi-vectored thrust airship. *22nd AIAA, Lighter-Than-Air Systems Technology Conference*. 22-26 June 2015, Dallas, TX, AIAA 2015–3228.

Chen L, Duan DP, Sun DS. Design of a multi-vectored thrust aerostat with a reconfigurable control system. *Aerospace Science and Technology*. 2016, 53:95–102.

Consolini L, Tosques M. A minimum phase output in the exact tracking problem for the nonminimum phase underactuated surface ship. *IEEE Transactions on Automatic Control*. 2012, 57(12):3174–3180

Do KD, Jiang ZP, Pan J. Robust global stabilization of under-actuated ships on a linear course. *Proceedings of the American Control Conference*. Anchorage, AK, 2002:304–309.

Fossen TI, Godhavn JM, Berge S, Lindegaard KP. Nonlinear control of underactuated ships with forward speed compensation. *Proc. 4th IFAC Symposium on Nonlinear Control Systems Design (NOLCOS'98)*. Enschede, The Netherlands, 1-3 July 1998:121–126.

Godhavn JM, Fossen TI, Berge SP. Non-linear and adaptive back-steping designs for tracking control of ships. *International Journal of Adaptive Control and Signal Processing*. 1998, 12:649–670.

Godhavn JM, Nonlinear tracking of underactuated surface vessels. *Proceedings of the 35th Conference on Decision and Control*. Kobe, Japan, December 1996:975–980.

Khoury GA, Gillett JD. Airship Technology. *Cambridge University Press, 1999*.

Lauvdal T, Fossen TI. Nonlinear rudder-roll damping of non-minimum phase ships using sliding mode control. *European Control Conference*. Brussels, Belgium, 1-4 July 1997:1689–1694.

Lekkas AM, Fossen TI. A time-varying look-ahead distance guidance law for path following. *9th IFAC Conference on Manoeuvring and Control of Marine Craft*. Arenzano, Italy, 19-21 September 2012:398–403.

Leonessa A, VanZwieten T, Morel Y. Neural network model reference adaptive control of marine vehicles. In *Current Trends in Nonlinear Systems and Control*. (Menini L, Zaccarian L, Abdallah CT, eds.), Birkhäuser, Boston, MA, 2006:421–440.

Morel Y, Leonessa A. Indirect adaptive control of a class of marine vehicles. *International Journal of Adaptive Control and Signal Processing*. 2010, 24:261–274.

Morel Y, Leonessa A. Adaptive nonlinear tracking control of an under-actuated non-minimum phase model of a marine vehicle using ultimate boundedness. *Proceedings of the 42nd IEEE Conference on Decision and Control*. Anchorage, AK, 2002:304–309.

Pettersen KY, Fossen TI. Underactuated dynamic positioning of a ship — experimental results. *IEEE Transactions on Control Systems Technology*. 2000, 8(5):856–863.

Pinkster JA, Marin UN. Dynamic positioning of large tankers at sea. *18th Annual Offshore Technology Conference*. Houston, TX, 5-8 May 1986:459–475.

Rooz N, Johnson EN. Design and modeling of an airship station holding controller for low cost satellite operations. *AIAA Guidance, Navigation, and Control Conference and Exhibit*. 15-18 August 2005, San Francisco CA, AIAA 2005–6200.

Slotine J, Li W. *Applied Nonlinear Control*. Prentice Hall, Englewood Cliffs, NJ, 1991.

Smith S, Fortenberry M, Lee M, Judy R. HiSentinel80: Flight of a high altitude airship. *19th AIAA Lighter-than-Air Technology Conference*. 20-22 September 2011, Virginia Beach, VA, AIAA 2011-6973

Toussaint GJ, Basar T, Bullo F. Tracking for nonlinear underactuated surface vessels with generalized forces. *Proceedings of the 2000 International Conference on Control Applications*. Anchorage, AK, 25-27 September 2000:355–360.

Yang Y, Yan Y. Backstepping sliding mode control for uncertain strict feedback nonlinear systems using neural-network-based adaptive gain scheduling. *Journal of Systems Engineering and Electronics*. 2018, 29:580–586.

Yang Y, Yan Y. Attitude regulation for unmanned quadrotors using adaptive fuzzy gain-scheduling sliding mode control. *Aerospace Science and Technology*. 2016, 54:208–217.

Zheng ZW, Wu Z. Global path following control for underactuated stratospheric airship. *Advances in Space Research*. 2013, 52:1384–1395.

Zheng ZW, Chen T, Xu M, Zhu, M. Modeling and path-following control of a vector-driven stratospheric satellite. *Advances in Space Research*. 2016, 57(9):1901–1913.

Yang YN. A time-specified nonsingular terminal sliding mode control approach for trajectory tracking of robotic airships. *Nonlinear Dynamics*. 2018, 92: 1359–1367.

Yang XX, Liu DN. Conceptual design of stratospheric airships focusing on energy balance. *Journal of Aerospace Engineering*. 2018, 31(2): 04017094-1–0401794-8.

Zhang JS, Yang XX, Deng XL. Tragectory control method of stratospheric airships based on model predictive control in wind field. *Proceedings of the Institution of Mechanical Engineers Part G, Journal of Aerospace Engineering*. DOI:10.1177/0954410017735128.

Degraded planetary tracking control of an omni-directional vectored-thruster aerostat

Chen, Li

2018-10-30

Chen L, Whidborne J, Dong Q, Duan D and Liu J., Degraded planetary tracking control of an omni-directional vectored-thruster aerostat, Journal of Aerospace Engineering, Volume 32, Issue 4, Article Number 04019026.

https://doi.org/10.1061/(ASCE)AS.1943-5525.0001005